PCCP

PAPER

View Article Online
View Journal | View Issue

Cite this: *Phys. Chem. Chem. Phys.*, 2019, **21**, 2365

Ultrafast internal conversion dynamics of bilirubin bound to UnaG and its N57A mutant†

Xiaodan Cao, [a] Changcheng Zhang,[d] Ziheng Gao,[d] Yangyi Liu,[a] Yuzheng Zhao,[d] Yi Yang, [d] Jinquan Chen, *[ae] Ralph Jimenez *[bc] and Jianhua Xu [ae]

Received 11th December 2018,
Accepted 16th January 2019

DOI: 10.1039/c8cp07553k

rsc.li/pccp

Fluorescent proteins (FPs) have become fundamental tools for live cell imaging. Most FPs currently used are members of the green fluorescent protein super-family, but new fluorophores such as bilin-FPs are being developed and optimized. In particular, the UnaG FP incorporates bilirubin (BR) as a chromophore, enhancing its fluorescence quantum yield by three orders of magnitude relative to that in solution. To investigate the mechanism of this dramatic enhancement and provide a basis for further engineering of UnaG and other tetrapyrrole-based fluorophores, we performed picosecond fluorescence and femtosecond transient absorption measurements of BR bound to UnaG and its N57A site-directed mutant. The dynamics of wt-UnaG, which has a fluorescence QY of 0.51, are largely homogeneous, showing an excited state relaxation of ~200 ps, and a 2.2 ns excited-state lifetime decay with a kinetic isotope effect (KIE) of 1.1 for D_2O *vs.* H_2O buffer. In contrast, for UnaG N57A (fluorescence QY 0.01) the results show a large spectral inhomogeneity with excited state decay timescales of 47 and 200 ps and a KIE of 1.4. The non-radiative deactivation of the excited state is limited by proton transfer. The loss of direct hydrogen bonds to the *endo*-vinyl dipyrrinone moiety of BR leads to high flexibility and structural heterogeneity of UnaG N57A, as seen in the X-ray crystal structure.

Introduction

Bilirubin (BR) is a linear tetrapyrrole chromophore which is produced in vertebrates by the degradation of heme, only differing by one double bond in the methylene bridge from its metabolic precursor, biliverdin (BV). Bilin-FPs such as UnaG, Sandercyanin, miRFPs, and smURFP are an emerging class of fluorophores due to their genetic encodability, potential for high brightness, photoswitching, and the far-red emission of BV.[1–5] In solvents at 300 K, BR does not fluoresce significantly (fluorescence quantum yields (QY) ~ 10^{-4}).[6] However, the BR-UnaG holoprotein (henceforth referred to as UnaG),[2] has a much higher QY (0.51) than is typical for other bilin-FPs, whose QY range from 0.016–0.18.[3–5] This 15.6 kDa protein contains a single BR in a nearly planar conformation with direct and water-mediated hydrogen-bonds to the both dipyrrinone moiety and propionates. The Asn57 sidechain stabilizes this conformation with hydrogen-bonding interactions to the *endo*-vinyl dipyrrinone moiety and the C-ring propionate (Scheme 1 left). The UnaG N57A point mutant, in which BR fluorescence is nearly quenched (QY 0.01), lacks all direct hydrogen-bonds in the *endo*-vinyl dipyrrinone moiety (Scheme 1 right) and shows a much larger torsion angle of the dipyrrinone A–B rings. Thus it appears that chromophore planarity and/or rigidity are key factors in enhancing the QY.

Although ultrafast time-resolved measurements of BR in proteins have not been reported yet, several studies report the characterization of BR bound to human serum albumin and in organic solvents.[7–10] Fluorescence up-conversion measurements by Zeitz and Gillbro provided the most direct measure of the BR excited state kinetics in solvents, revealing picosecond decay timescales.[9] They suggest that deactivation in the internally H-bonded BR in $CHCl_3$ is highly efficient due to a conical intersection (CI) near the Franck–Condon region, or due to excited-state proton transfer (ESPT). The latter mechanism is predicted by a recent theoretical study.[11] Although ESPT can generate new products that yield dual emission with large Stokes shift or red-shifted emission as observed in GFP,[12–14] it also can become

[a] *State Key Laboratory of Precision Spectroscopy, East China Normal University, Shanghai, China. E-mail: jqchen@lps.ecnu.edu.cn*
[b] *JILA, NIST and University of Colorado, Boulder, USA. E-mail: rjimenez@jila.colorado.edu*
[c] *Department of Chemistry and Biochemistry, University of Colorado, Boulder, CO, USA*
[d] *School of Pharmacy, East China University of Science and Technology, Shanghai, China*
[e] *Collaborative Innovation Center of Extreme Optics, Shanxi University, Taiyuan, Shanxi 030006, China*

† Electronic supplementary information (ESI) available: Data analysis methods; Fig. S1–S12 showing additional time resolved fluorescence and transient absorption results, and the crystal structure of the subunits for UnaG N57A; Tables S1–S8 showing the corresponding fitting parameters for these data, and the crystal structure parameters for wt-UnaG and UnaG N57A. See DOI: 10.1039/c8cp07553k

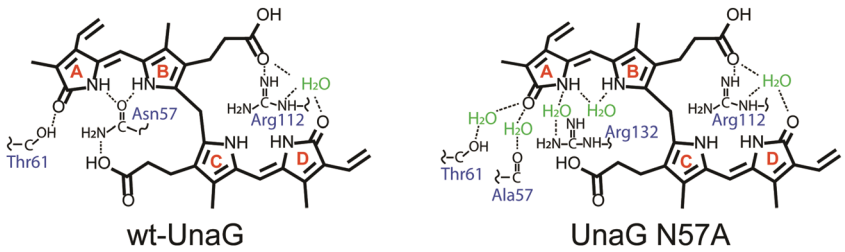

Scheme 1 Chromophore binding-site interactions with BR in wt-UnaG and UnaG N57A (PDB ID: 4I3B, 4I3D).

an excited-state deactivation channel by routing population through a conical intersection, especially for pyrroles.[15,16] For bilin-FPs, ESPT is the usual deactivation pathway from the excited state to ground state.[3,17–20] As for BV, femtosecond spectroscopy of the chromophore in solution has not yet been reported, but investigations of BV-containing near-IR FPs engineered from bacteriophytochromes (Bphs) and cyanobacterial phytochromes (Cphs) have been extensively investigated, revealing excited state dynamics with ESPT and/or isomerization and a diverse range of excited state lifetimes, twist motions, hydrogen bonding interactions, spectral heterogeneities and fluorescence quantum yields.[3,17–20]

Here, we present the first femtosecond transient absorption and picosecond fluorescence measurements on the highly fluorescent wild-type UnaG and the quenched N57A mutant to reveal the photocycle of the bound BR chromophore, including spectral properties, proton transfer process, and the sidechain interactions. We discover that direct hydrogen bonds to BR ring A and B provided by N57 and T61 sidechains in wt-UnaG inhibit deactivation of the initial populated bright state to the less emissive intermediate states and ultimately lead to the high fluorescence QY. Our results may facilitate engineering of brighter and more functional BR-based FPs.

Experimental methods

Sample preparation

The proteins (wild type UnaG and UnaG N57A mutant) are provided by Prof. Yi Yang's group base on the method reported by Kumagai *et al.*[2] Bilirubin (Sigma-Aldrich, 98% purity) was dissolved in DMSO as stock solution (2 mM). The bilirubin/UnaG complex were prepared at 2 : 1 molar ratio in Tris buffer (50 mM Tris–HCl and 150 mM NaCl, pH 7.4), and then purified with PD G-25 columns (GE Healthcare) to remove free bilirubin and DMSO.

Spectroscopy measurements

Steady-state absorption spectra and fluorescence spectra were recorded on a UV-Vis spectrophotometer (TU1901, Beijing Purkinje General Instrument Co. Ltd) and FluoroMax-4 spectrofluorometer (Horiba, Jobin Yvon), respectively. Transient absorption (TA) spectra over the 350 to 720 nm spectral range were acquired on a transient absorption spectrometer (Helios-EOS fire, Ultrafast System), and 1 kHz Ti:sapphire amplifier system with 120 fs time resolution. The 490 nm pump pulse energy was limited to 100 nJ. Fluorescence lifetimes were measured on a home-built time-correlated single photon counting (TCSPC) system. The excitation pulse was provided by a picosecond super-continuum fiber laser (SC400-pp-4, Fianium, UK) with a repetition rate of 20 MHz, and the fluorescence was recorded by a TCSPC module (PicoHarp 300, PicoQuant) and a MCP-PMT (R3809U-50, Hamamatsu). A monochromator (7ISW151, Sofn Instruments) was used to select the emission wavelength.

Results and discussion

Wild type UnaG

UV-Vis absorption and emission spectra of wild type UnaG (henceforth we denote as wt-UnaG) in Tris buffer (50 mM Tris–HCl with 150 mM NaCl, pH 7.4) show peaks around 496 nm and 530 nm respectively (Fig. 1A), which is consistent with previous results.[2] Isotropic fluorescence decay at 530 nm from time-correlated single photon counting (TCSPC) measurements with 80 ps time resolution reveals a single exponential decay with 2.2 ns time constant (Fig. 1B and Table 1). TCSPC anisotropy measurements on wt-UnaG in buffer (Fig. S1, ESI† green dots) reveal a ~11 ns decay. This timescale is consistent with overall rotational tumbling of the protein, as confirmed by the increase in time constant to ~84 ns in a higher viscosity buffer (with 50% glycerol, Fig. S1, ESI† pink dots). The overall tumbling time of similar-sized proteins is reported to be ~10 ns

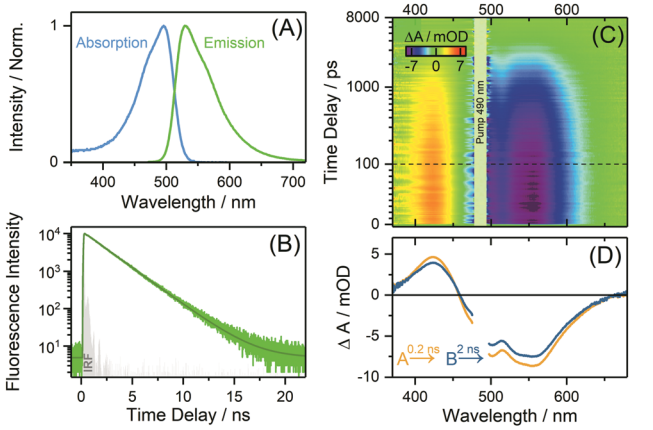

Fig. 1 Spectral properties of wt-UnaG in Tris buffer. (A) Absorption and emission spectra. (B) Isotropic time resolved fluorescence from TCSPC measurement (490 nm excitation and 530 nm detection). (C) Broadband transient absorption spectra and (D) corresponding EADS from global fitting.

Table 1 wt-UnaG TCSPC time constants

Buffer	QY	TCSPC lifetime (ns)	k_{EXC} (s^{-1})	k_{RAD} (s^{-1})	k_{NR} (s^{-1})
H_2O Tris buffer	0.51	2.21 (χ^2 = 1.17)	4.5×10^8	2.3×10^8	2.2×10^8
D_2O Tris buffer	0.56	2.41 (χ^2 = 1.19)	4.1×10^8	2.3×10^8	1.8×10^8
H_2O Tris with 6.7% glycerol	0.51	2.20 (χ^2 = 1.20)	4.5×10^8	2.3×10^8	2.2×10^8

for myoglobin (16.7 kDa) and 8.7 ns for lysozyme (14.3 kDa),[21–23] indicating that wt-UnaG (19 kDa with affinity tags for purification) is monomeric under these conditions.

Broadband femtosecond transient absorption (TA) measurements with 120 fs time resolution (Fig. 1C) show a stimulated emission (SE) band around 550 nm, an excited-state absorption (ESA) band around 425 nm, and a ground state bleach (GSB) band near 500 nm. These bands decay without any change of the peak positions (Fig. S2, ESI†). Global analysis followed by singular value decomposition (SVD) process was performed in Surface Xplorer software (Ultrafast Systems, Inc.). One component with a time constant of 1.9 ns fits well with the principal SVD kinetics, but two components with time constants of 2.0 ns and 0.2 ns (Table S1, ESI†) produce an even better fit, where the 0.2 ns component only shows a small negative band with a peak around 500 nm in the decay-associated spectra (DAS, Fig. S3, ESI†). The 2.0 ns component from global analysis likely corresponds to the 2.2 ns lifetime from time-resolved fluorescence, representing the decay of the BR excited state. Both TA and TCPSC decays at 550 nm are well fitted by single exponential decay, whereas TA signal at 504 nm and TCSPC signal at 500 nm requires two exponentials fits (Fig. S4 and Tables S2, S3, ESI†). This implies that the 0.2 ns component only appears on the blue side of the SE band and it is likely due to a spectral narrowing of the SE band, which indicates excited state structural relaxation of BR in protein environment. Evolution-associated difference spectra (EADS) with a sequential model (Fig. 1D) show the two components have similar spectra. The EADS method has often been used to analyze the dynamics of protein photocycles.[17–20,24] The first EADS corresponds to the time-zero difference spectrum, which evolves into the second EADS with time constant τ_1, and so on. In this analysis, an overall loss of GSB, ESA and SE features corresponds to excited state decay, whereas spectral evolution without loss of excited state population is attributed to the relaxation process in the excited state. In addition, the global analysis indicates that no long-lived species are formed in wt-UnaG (*i.e.* no isomerization occurs). The single exponential decay of the excited state population and the TA results indicate that wt-UnaG is spectrally homogenous.

To examine the possibility of ESPT in wt-UnaG, experiments were performed in D_2O Tris buffer. Fluorescence and TCSPC measurements show increased fluorescence intensities (QYs from 0.51 to 0.56) and longer lifetimes (from 2.2 ns to 2.4 ns) in 90% D_2O Tris buffer compared to H_2O Tris buffer (Fig. 2 and Table 1). Calculations of the radiative and non-radiative rates (method in ESI†) demonstrate that the increase in excited-state lifetime and QY in D_2O Tris buffer is due to the decrease in the non-radiative rate while the radiative rate is constant. A control experiment was performed with addition of 6.7% glycerol in

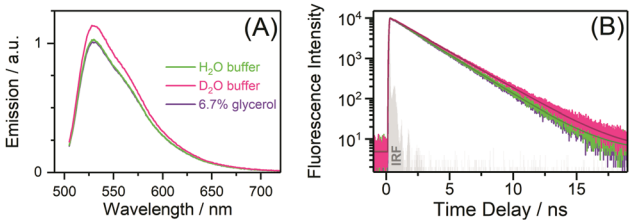

Fig. 2 Isotope effects of wt-UnaG. (A) Emission spectra of wt-UnaG in H_2O Tris buffer, D_2O Tris buffer and H_2O Tris buffer with 6.7% glycerol. (B) Time-resolved fluorescence decays of wt-UnaG in the same three buffers (excitation at 496 nm and detection at 530 nm). Fitting results are listed in Table 1.

H_2O Tris buffer (Fig. 2 purple lines), which has the same viscosity as D_2O Tris buffer, showing the increased lifetime is not due to viscosity effects. Moreover, TA measurements of wt-UnaG in D_2O buffer showed similar increase in lifetimes as seen in TCSPC (Fig. S3B, S5 and S6, ESI†). As the structure of BR in protein is unchanged due to the identical absorption and emission spectra, and the increase in QY and lifetime is due to the decrease in non-radiative decay rate, we believe it should be assigned to a proton-motion mediated process since it is a common non-radiative decay pathway for bilin's excited states. However, this process in wt-UnaG is not a dominant non-radiative pathway, so the KIE is rather small in wt-UnaG.

The photophysical model for wt-UnaG is straightforward as illustrated in Scheme 2. The BR chromophore shows a single exponential decay of excited state, and the radiative decay with a rate of 2.3×10^8 s^{-1} (τ_{RAD} = 4.3 ns) is the main channel that accounts for 51% of the excited state decay. The structural relaxation in the excited state shows a relatively long timescale of 200 ps. The small KIE of 1.1 in wt-UnaG demonstrates that ESPT is a minor contribution to the deactivation of BR's excited state. The high QY, long excited state lifetime, small KIE and

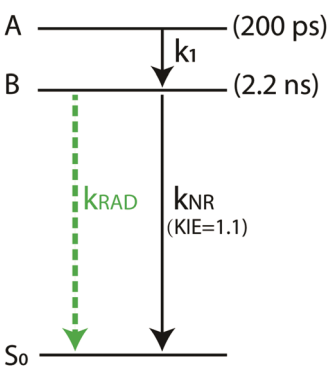

Scheme 2 Excited state dynamics model for BR in wt-UnaG.

absence of isomerization indicate that the binding site in wt-UnaG provides a rigid environment for BR.

The UnaG N57A mutant

UnaG N57A shows a broader absorption in the red edge (Fig. 3A blue solid line) and a red-shifted as well as much broader emission (Fig. 3A green solid line, with a peak around 542 nm) compared to wt-UnaG (Fig. 3A dashed lines). Isotropic fluorescence decay from TCSPC measurements reveal a much faster decay with multi-exponential of 50, 190 and 930 ps time constant (Fig. 3B and Table 2). TCSPC anisotropy measurements on UnaG N57A in Tris buffer (Fig. S7, ESI† blue dots) reveal the same decay timescale seen for wt-UnaG, suggesting that it is also monomeric.

Compared to wt-UnaG, femtosecond TA measurements of UnaG N57A with 120 fs time resolution within a 1 ns time window shows a similar ESA peak around 425 nm and a GSB peak around 500 nm as in wt-UnaG, but a different SE feature around 560 nm (Fig. 3C). The peaks of SE band red-shift from 557 nm to 580 nm in the first 30 picoseconds, and then blue shift to ~570 nm on longer timescales (Fig. S8, ESI†). The SE kinetics at 560 nm are much faster than the GSB recovery at 502 nm (Fig. S9, ESI†), thus pointing to the presence of intermediate states before repopulation of the ground state. Global analysis was carried out to determine the number of excited states and EADS analysis with a sequential model was performed to visualize the evolution of the excited and intermediate states of the system. Four components are required in the global analysis, with lifetimes of 370 fs, 4.3 ps, 47 ps and 200 ps (Table S4, ESI†), and the corresponding EADS was shown in Fig. 3D. The first EADS (pink) with 370 fs shows an ESA band around 430 nm, a GSB band around 500 nm and a SE band around 553 nm. It interconverts into the second EADS (yellow) without loss of GSB and ESA but with a red shift of the SE band to 565 nm. The second EADS interconverts into the third EADS (cyan) with a lifetime of 4.3 ps, also without loss of GSB but further red shift of SE band to 582 nm. The third EADS (cyan) decays with a lifetime of 47 ps and shows an overall loss of GSB and ESA, and the fourth EADS (purple) shows a minor excited state decay with a lifetime of 200 ps and SE peaks around 568 nm. Since the spectra of the 370 fs and 4.3 ps components do not show loss of GSB features, they are likely to be the result of excited-state structural relaxation of BR. On the other hand, the 47 ps and 200 ps time scales, which closely correspond to time constants from TCSPC, represent the loss of excited state population.

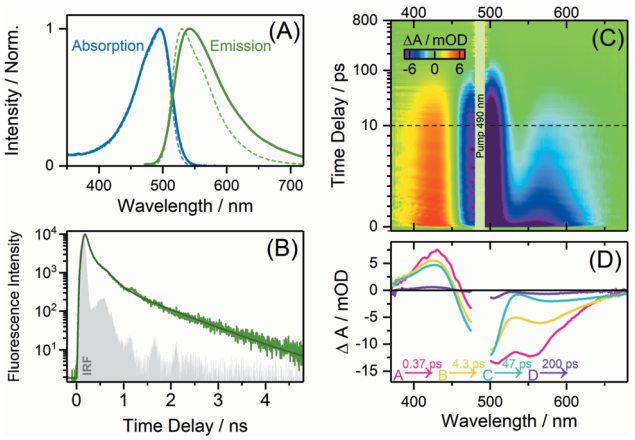

Fig. 3 Spectral properties of UnaG N57A in Tris buffer. (A) Absorption and emission spectra of UnaG N57A (solid lines) and compared to wt-UnaG (dashed lines). (B) Isotropic time resolved fluorescence from TCSPC measurement (490 nm excitation and 540 nm detection). (C) Broadband transient absorption spectra and (D) corresponding EADS from global fitting.

The excited state dynamics of UnaG N57A shows a few unusual features. First, the 200 ps component of the EADS, has a more blue-shifted SE peak than the 47 ps EADS component. It is difficult to reconcile a typical excited state relaxation process with the observed blue shifted emission of the longest lifetime component. Furthermore, a 47 ps rise time was not observed in any of the kinetics. Thus, the species with a 200 ps lifetime is not produced on the 47 ps timescale of the third component. We therefore infer that these two excited-state components reflect pre-existing ground state species, likely originating from structural heterogeneity in the ground state (discussed below). This spectral inhomogeneity is also clear in the DAS (Fig. S10, ESI†) which show different amplitudes and maxima of the SE, GSB and ESA bands. A similar case was reported for BV in RpBphP2 which shows a biexponential excited state decay with 43 ps and 170 ps time constants, arising from structural heterogeneity in the Pr ground state.[17] Moreover, this structural heterogeneity of PCB in cyanobacterial phytochrome Cph1 is also widely observed with time-resolved spectroscopy.[25–27]

A second observation is that EADS reveal the contribution of SE relative to GSB decreases at long times (Fig. 3D), which indicates that BR converts to dark states during the excited-state relaxation. Similar dynamics were noted for BR in organic solvents, where it is seen that BR is highly fluorescent near the Franck–Condon region, with a 350 fs lifetime, but it then converts to dark intermediates on an ultrafast timescale, then finally decays to the ground state in 15 ps.[10,22] Similarly, state A in UnaG N57A with 370 fs lifetime can be attributed to a bright state near the Franck–Condon region, and the subsequent states show progressively less emission (smaller amplitude SE features). In addition, although an upcoming ESA band compensating the SE amplitude could also cause the decrease in SE, the rise of an ESA band is usually accompanied by formation of new species such as isomerization. However, no formation of long-lived species is observed that bring about new ESA bands.

Steady state emission, TCSPC and TA measurements on UnaG N57A in D_2O Tris buffer revealed significant isotope effects, including a 1.62-fold increase in fluorescence intensity (Fig. 4A) and slower fluorescence decay timescales (Fig. 4B and Table 2). The control experiment in 6.7% glycerol/Tris buffer (Fig. 2 purple lines) showed that this increase is not mainly due to viscosity effects. TA measurements in 80% D_2O Tris buffer (Fig. S12, ESI†) show clear effects at some wavelengths. For example, the kinetic trace at 502 nm of the GSB band (Fig. 4C) shows a half-life of 46 ps in H_2O Tris buffer and 73 ps in 80% D_2O Tris buffer (1.59 fold). However, kinetic trace at 560 nm of the SE band

Table 2 UnaG N57A TCSPC time constants

Buffer	QY	τ_1 (ns)	τ_2 (ns)	τ_3 (ns)	$\sum \alpha_i \tau_i$ (ns)	χ^2
H_2O Tris buffer	0.010	0.05 (76%)	0.19 (21%)	0.93 (3%)	0.11	1.10
D_2O Tris buffer	0.016	0.07 (73%)	0.28 (23%)	1.17 (4%)	0.16	1.25
H_2O Tris with 6.7% glycerol	0.011	0.05 (76%)	0.20 (21%)	0.94 (3%)	0.11	1.10

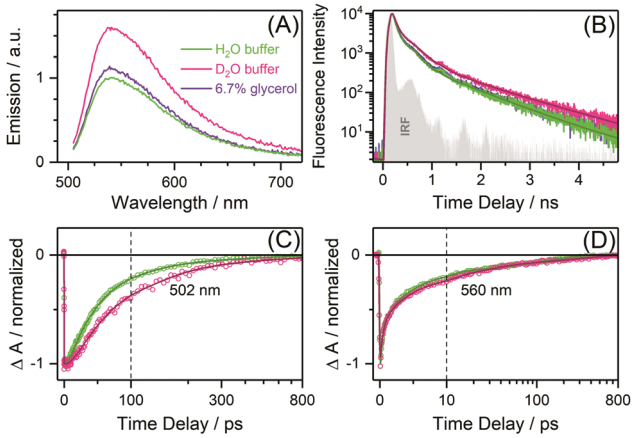

Fig. 4 Isotope effects on dynamics of UnaG N57A. (A) Emission spectra of UnaG N57A in H_2O Tris buffer, D_2O Tris buffer and H_2O Tris buffer with 6.7% glycerol. (B) Time-resolved fluorescence decays of UnaG N57A in the same three buffers (excitation at 496 nm and detection at 540 nm). Fitting results are listed in Table 2. (C) Normalized TA kinetics of UnaG N57A at 502 nm (GSB) and (D) at 560 nm (SE) in H_2O-Tris buffer and D_2O-Tris buffer. Fitting results are listed in Table S5 (ESI†).

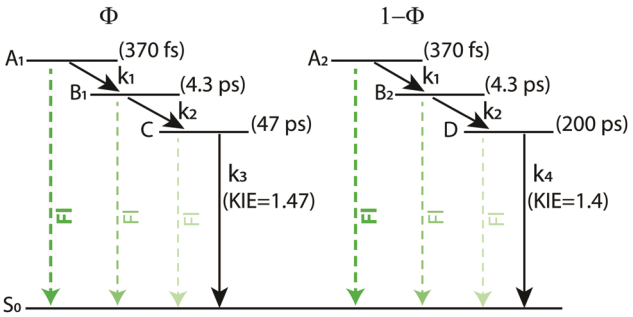

Scheme 3 Excited state dynamics model for BR in UnaG N57A. A is a bright state, and the later are darker states. C and D are conformers that exist in ground state due to structural heterogeneity. The values of k_1 = (0.37 ps)$^{-1}$ and k_2 = (4.3 ps)$^{-1}$ are the same in both cases, but k_3 = (47 ps)$^{-1}$ and k_4 = (200 ps)$^{-1}$ are different. Decays to the ground state are rate-limited by proton transfer.

doesn't show significant KIE effect (Fig. 4D). Global fitting results (Table S4, ESI†) show that the 0.37 ps and 4.3 ps components are nearly the same for H_2O and D_2O, whereas the 47 ps and 200 ps components increase to 69 ps (1.47 fold) and 280 ps (1.4 fold) respectively. This increase is consistent with TCSPC measurements (Table 2). These results demonstrate that proton transfer is rate-limiting in the decay of the excited state but not for structural relaxation within the excited state. Thus, a KIE is observed in the GSB kinetics but not in the SE kinetics. This is because the SE signal from TA measurement is predominantly from the bright states A (46%) and B (42%) that do not participate in ESPT, whereas states C and D which do participate in ESPT are only weakly emissive. Moreover, the significant KIE observed in TCSPC measurements originates from the lowest excited states (C and D) while the ultrafast dynamics is beyond the experimental time resolution.

The photophysical model for N57A (Scheme 3) requires the consideration of heterogeneous excited-state kinetics, which we represent with two populations with fractions Φ and $1 - \Phi$. Excitation of BR reaches a highly fluorescent state A near the Franck–Condon region, which relaxes to state B with on a 370 fs timescale. State B, with a red shift of 15 nm, is less emissive and it relax to the lowest excited state C or D on a 4.3 ps time scale. States C and D, with peak around 582 nm and 568 nm, are even less emissive than their precursors, and relax to the ground state with 47 ps and 200 ps timescales, respectively. The rate of proton transfer limits the deactivation of states C and D to the ground state. As suggested by Toh *et al.* for BV in bacteriophytochromes,[17] the reverse proton transfer rate in the ground state (not shown) is likely to be very fast and therefore no ground-state intermediates are accumulated or observed.

Chromophore binding-site interactions

To understand the molecular origins of the differences in excited state dynamics between wt-UnaG and N57A, the crystal structures were examined. Since the two propionates of BR are not in the same plane with the pyrrole rings and the π-electron conjugation does not extend to the two propionates, we focus on the four pyrrole rings.

The structure of wt-UnaG (Fig. 5, green) shows three direct hydrogen bonds to the *endo*-vinyl dipyrrinone moiety provided by N57 and T61 sidechains, one water-mediated hydrogen bond to ring D carbonyl, and two π–π interactions between ring D and R112, ring B and R132 respectively, interacting with BR. The sidechain of T61 provides a hydrogen bond to the BR ring A carbonyl with an average distance of 2.6 Å, and N57 interacts with the nitrogen of the pyrrole ring A and B with average distances of 2.9 Å and 3.0 Å (Table S7, ESI†). Spectroscopic studies of BV in bacteriophytochromes have shown that the strength of hydrogen bonding to the pyrrole ring carbonyl determines excited-state lifetime, Lumi-R quantum yield and spectral heterogeneity.[24] The presence of these interactions in wt-UnaG most likely explains the long lifetime, spectral homogeneity and absence of photoisomerization. At the other end of the BR chromophore, the structure shows a single water-mediated hydrogen bond to the carbonyl group of ring D, and the distance for a possible π–π interaction between ring D and R112 is 3.4 Å. The ~200 ps relaxation process observed in wt-UnaG can be assigned to the structural distortion of ring D instead of a more

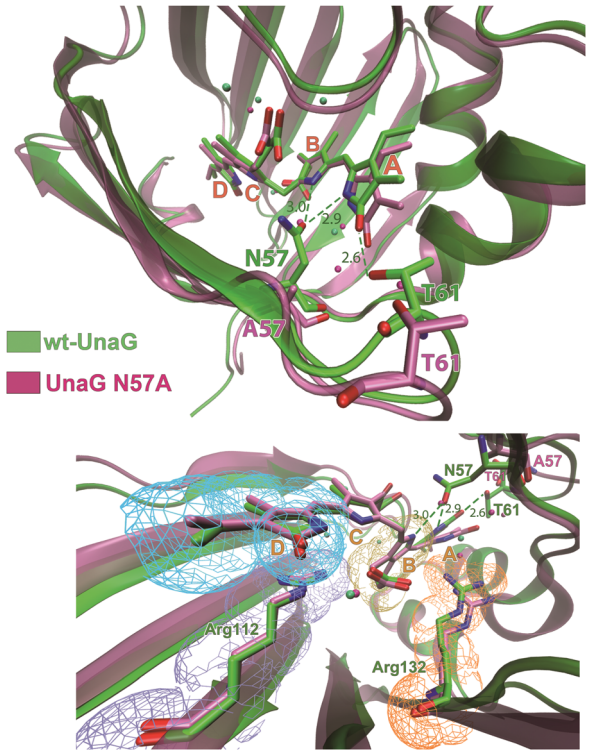

Fig. 5 Structures of wt-UnaG (PDB 4I3B) and UnaG N57A (PDB 4I3D). Direct hydrogen bonds to the four pyrrole rings are shown with dashed lines, π–π interactions between ring D-Arg112, ring B-Arg132 are shown with van der Waals surfaces by mesh, waters within 3 Å of BR are shown by spheres.

rigid ring A. Moreover, we conjecture that mutations that provide strong hydrogen bonding to the ring D carbonyl could result in an even higher fluorescence QY. As pyrroles are known to deprotonate in the excited state,[15,16] the ESPT process in wt-UnaG most likely occurs through a hydrogen bond from the nitrogen of ring A or B to N57 subsequent to a structural distortion of the chromophore and/or binding site perhaps propagating from ring D.

In UnaG N57A (Fig. 5, magenta) with quenched fluorescence (QY 0.01), the point mutation removes two direct hydrogen bonds to the nitrogen of pyrrole rings A and B, and also leads to the rearrangement of nearby residues that results in the loss of the hydrogen bond between T61 and ring A carbonyl. These direct hydrogen bonds are replaced with water-mediated hydrogen-bonds. Moreover, the π–π interaction between ring B and R132 is also lost. These modifications increase the overall flexibility of BR and permit a much larger torsion angle of the dipyrrinone A–B rings. The spectral inhomogeneity, including a broader absorption at the red edge and broader emission spectra compared to wt-UnaG, likely originate from the distinct ground state subpopulations as seen in the diversity of torsional angles and hydrogen bond interactions within the four subunits from the crystal structure (Fig. S11 and Tables S6, S7, ESI†). We suggest that spectral state C with 47 ps lifetime and red-shifted emission originates from a subpopulation with large torsional angles and weak hydrogen bonding. In the absence of direct side-chain to BR hydrogen bonding to hinder the twist motion, proton transfer from the nitrogen of ring A or B to hydrogen bonded waters is more easily triggered by the distortion of ring A. In contrast, we suggest that state D with 200 ps lifetime and blue-shifted emission arises from a subpopulation with smaller torsional angles that more closely resemble the conformation of BR in wt-UnaG. Temperature-dependent studies would be informative for a deeper investigation of these dynamics.

Comparison to ultrafast dynamics of other bilin-based fluorescent proteins

As our study represents the first ultrafast spectroscopy investigations of a natural BR-binding protein, we place our results in the context of investigations of other bilin-based FPs in which the competition between fluorescence, proton-transfer, and photoisomerization has been considered. The photophysical consequences of the high flexibility and structural heterogeneity of UnaG N57A are similar to what has been observed in other bilin-based FPs.[17,24,28] For example, the RpBphP2 also showed bi-exponential excited state decay of 43 and 170 ps which arises from structural heterogeneity of BV in the Pr ground state.[17] A Pr ground state heterogeneity that results in spectral heterogeneity is also reported in Cph1Δ which has distinct reaction rates in the excited states of PCB.[25] Wild-type SaBphP1 showed spectral heterogeneity attributed to different hydrogen bond isoforms in the absence of hydrogen bonding to the carbonyl group of ring D of BV chromophore, while its T289 mutant is less heterogeneous when a hydrogen bond is introduced at this position.[24,26]

ESPT is frequently invoked as an excited-state deactivation pathway in bilin-FPs.[3,17–20] For example, iRFPs that are derived from BphPs showed increased QY and excited state lifetimes in D_2O buffer (KIE as high as 1.8), suggesting that ESPT is still the dominant nonradiative pathway even though these proteins have been engineered for higher fluorescence QYs (as high as 13%) for use as genetically-encoded fluorophores.[19,20] The dynamics of wt-UnaG resembles those of the iRFPs in that the binding site effectively restricts bilin chromophore photoisomerization, but the reduced KIE in wt-UnaG and concomitant restriction of the proton transfer process results in a significantly larger fluorescence QY.

Conclusions

We find the rigid environment for BR in wt-UnaG provided by direct sidechain–chromophore interactions results in the highest QY (0.51) and longest excited state lifetime (2.2 ns) than other bilin-based FPs, where ESPT is a minor deactivation pathway. In contrast, the N57A point mutation leading to the loss of all direct hydrogen bonds to *endo*-vinyl dipyrrinone moiety of BR and their replacement with hydrogen-bonding to water results in increased flexibility and structural heterogeneity with excited state lifetimes of 47 and 200 ps. This flexibility permits conversion to less emissive states and also enables proton transfer. Strategies for enhancing the fluorescence of BR-based FPs should focus on providing a more rigid environment

by introducing direct hydrogen bonds to fix the excited-state chromophore and its hydrogen-bonding network near configurations with strong Franck–Condon overlap with the ground state.

Conflicts of interest

There are no conflicts to declare.

Acknowledgements

This study was funded by National Natural Science Foundation of China (No. 11674101, 21873030 and 91850202 to J. C.) and the National Science Foundation Physics Frontier Center at JILA (NSF PHY 1734006 to R. J.). Supported by the 111 Project (B12024). R. J. is a staff member in the Quantum Physics Division of NIST. Certain commercial equipment, instruments, or materials are identified in this paper in order to specify the experimental procedure adequately. Such identification is not intended to imply that the materials or equipment identified are necessarily the best available for the purpose.

References

1 A. Miyawaki, *Nat. Methods*, 2016, **13**, 729–730.
2 A. Kumagai, R. Ando, H. Miyatake, P. Greimel, T. Kobayashi, Y. Hirabayashi, T. Shimogori and A. Miyawaki, *Cell*, 2013, **153**, 1602–1611.
3 S. Ghosh, C.-L. Yu, D. J. Ferraro, S. Sudha, S. K. Pal, W. F. Schaefer, D. T. Gibson and S. Ramaswamy, *Proc. Natl. Acad. Sci. U. S. A.*, 2016, **113**, 11513–11518.
4 E. A. Rodriguez, G. N. Tran, L. A. Gross, J. L. Crisp, X. Shu, J. Y. Lin and R. Y. Tsien, *Nat. Methods*, 2016, **13**, 763–769.
5 D. M. Shcherbakova, M. Baloban, A. V. Emelyanov, M. Brenowitz, P. Guo and V. V. Verkhusha, *Nat. Commun.*, 2016, **7**, 12405.
6 S. E. Braslavsky, A. R. Holzwarth and K. Schaffner, *Angew. Chem., Int. Ed.*, 1983, **22**, 656–674.
7 B. I. Greene, A. A. Lamola and C. V. Shank, *Proc. Natl. Acad. Sci. U. S. A.*, 1981, **78**, 2008–2012.
8 B. Zietz, A. N. Macphersona and T. Gillbro, *Phys. Chem. Chem. Phys.*, 2004, **6**, 4535–4537.
9 B. Zietz and T. Gillbro, *J. Phys. Chem. B*, 2007, **111**, 11997–12003.
10 C. Carreira-Blanco, P. Singer, R. Diller and J. L. P. Lustres, *Phys. Chem. Chem. Phys.*, 2016, **18**, 7148–7155.
11 H. P. Upadhyaya, *J. Phys. Chem. A*, 2018, **122**, 9084–9092.
12 V. I. Tomin, A. P. Demchenko and P.-T. Chou, *J. Photochem. Photobiol., C*, 2015, **22**, 1–18.
13 A. P. Demchenko, K.-C. Tang and P.-T. Chou, *Chem. Soc. Rev.*, 2013, **42**, 1379–1408.
14 M. Chattoraj, B. A. King, G. U. Bublitz and S. G. Boxer, *Proc. Natl. Acad. Sci. U. S. A.*, 1996, **93**, 8362–8367.
15 Z. Lan, L. M. Frutos, A. L. Sobolewski and W. Domcke, *Proc. Natl. Acad. Sci. U. S. A.*, 2008, **105**, 12707–12712.
16 O. David, C. Dedonder-Lardeux, C. Jouvet, H. Kang, S. Martrenchard, T. Ebata and A. Sobolewski, *J. Chem. Phys.*, 2004, **120**, 10101–10110.
17 K. C. Toh, E. A. Stojković, I. H. M. van Stokkum, K. Moffat and J. T. M. Kennis, *Proc. Natl. Acad. Sci. U. S. A.*, 2010, **107**, 9170–9175.
18 K. C. Toh, E. A. Stojković, I. H. M. van Stokkum, K. Moffat and J. T. M. Kennis, *Phys. Chem. Chem. Phys.*, 2011, **13**, 11985–11997.
19 J. Zhu, D. M. Shcherbakova, Y. Hontani, V. V. Verkhusha and J. T. M. Kennis, *Sci. Rep.*, 2015, **5**, 12840.
20 Y. Hontani, D. M. Shcherbakova, M. Baloban, J. Zhu, V. V. Verkhusha and J. T. M. Kennis, *Sci. Rep.*, 2016, **6**, 37362.
21 D. S. Gottfried, A. Kagan, B. M. Hoffman and J. M. Friedman, *J. Phys. Chem. B*, 1999, **103**, 2803–2807.
22 L. Luo, C.-H. Chang, Y.-C. Chen, T.-K. Wu and E. W.-G. Diau, *J. Phys. Chem. B*, 2007, **111**, 7656–7664.
23 R. Irwin and J. E. Churchich, *J. Biol. Chem.*, 1971, **246**, 5329–5334.
24 T. Mathes, J. Ravensbergen, M. Kloz, T. Gleichmann, K. D. Gallagher, N. C. Woitowich, R. St. Peter, S. E. Kovaleva, E. A. Stojković and J. T. M. Kennis, *J. Phys. Chem. Lett.*, 2015, **6**, 239–243.
25 P. W. Kim, N. C. Rockwell, S. S. Martin, J. C. Lagarias and D. S. Larsen, *Biochemistry*, 2014, **53**, 2818–2826.
26 C. Song, G. Psakis, C. Lang, J. Mailliet, W. Gärtner, J. Hughes and J. Matysik, *Proc. Natl. Acad. Sci. U. S. A.*, 2011, **108**, 3842–3847.
27 P. W. Kim, N. C. Rockwell, L. H. Freer, C.-W. Chang, S. S. Martin, J. C. Lagarias and D. S. Larsen, *J. Phys. Chem. Lett.*, 2013, **4**, 2605–2609.
28 X. Yang, J. Kuk and K. Moffat, *Proc. Natl. Acad. Sci. U. S. A.*, 2008, **105**, 14715–14720.